

Smart Bandage with Inductor-Capacitor Resonant Tank Based Printed Wireless Pressure Sensor on Electrospun Poly-L-Lactide Nanofibers

Fatemeh Nikbakhtnasrabadi, Ensieh S. Hosseini, Saoirse Dervin, Dhayalan Shakthivel, and Ravinder Dahiya*

Easy to use multifunctional wearable devices, with no wires hanging around, are needed for real time health monitoring at user's comfort. Herein, an inductor-capacitor (LC) resonant tank-based wireless pressure sensor, screen-printed on an electrospun Poly-L-lactide (PLLA) nanofibers-based flexible, biocompatible, and piezoelectric substrate is presented. The printed resonant tank (resonant frequency of ≈ 13.56 MHz) consists of a planar inductor connected in parallel with an interdigitated capacitor. The capacitance, of the interdigitated capacitor present on the piezoelectric substrate varies in response to applied pressure. As a result, the resonant frequency changes and the LC tank works as a wireless pressure sensor. The sensor exhibited high sensitivity 0.035 kPa^{-1} and 1200 Hz kPa^{-1} in wireless operation with excellent durability (over 1800 cycles). The sensitivity is the highest (1.75-fold higher) among printed wireless pressure sensors reported so far. Finally, the presented LC tank-based pressure sensor is integrated on a compression bandage to demonstrate its potential use in the online monitoring of sub-bandage pressure. The application of optimum pressure by the bandage, together with the electroceutical arrangement facilitated by the piezoelectric PLLA substrate, can accelerate the cell regeneration and hence wound healing.

in many ways advantageous compared to the matured silicon-based technology. For example, high temperature process steps are incompatible with flexible substrates (e.g., polyethylene terephthalate (PET), polyethylene naphtholate (PEN), and Polydimethylsiloxane (PDMS), etc.), which are typically needed in emerging applications such as electronic skin,^[1,5] and smart packages.^[6] Several flexible wearable sensors have been developed on such substrates for biomedical applications to monitor parameters, such as sweat pH,^[7] temperature,^[8] humidity,^[9] etc. Likewise, various force and pressure sensors have been developed to monitor physiological parameters such as blood pressure, respiration, and heart rate, etc.^[10–14]

It is preferable to have wireless data transmission from such sensors, as commonly employed hard wired approach does not consider user comfort. Therefore, the advanced technologies in this field aim to develop biocompatible and light weight


wearable sensors with fully integrated wireless system capable of continuous monitoring of physiological parameters. In this regard, Radiofrequency Identification (RFID) sensor tags are attractive as they eliminate the use of battery and the complexity of wired electronics.^[15,16] These tags are generally designed for high-frequency range (HF) 13.56 MHz band and ultrahigh frequency (UHF) range (860–960 MHz band depending on local regulations). However, with human body acting as a lossy medium with a high dielectric constant, the performance of RFID tags deteriorates when they are used for wireless epidermal sensing.

In contrast to far field-based systems, the HF band (3–30 MHz) allows devices to communicate through an inductive coupling in the near field region without emitting energy in far field. This short-range system is a promising alternative to transmit power and data where the medium is highly lossy for instance, human tissue. Most commercial sensing tags include a chip to store and process the RF signal, whereas in chipless tags no electronic components are included.^[16,17] LC circuit working in HF region can be used as a nondestructive sensing platform in biomedical applications, especially as an implant.^[18,19] Motivated by the above challenges, herein we have used the LC tank-based approach for wireless sensing.

1. Introduction

The progress in printed sensors and electronics in recent years have facilitated the development of electronics in flexible form factors and triggered advances in many application areas, such as wearable electronics, health monitoring, robotics, and interactive systems etc.^[1–4] These advances have also led to new materials and resource-efficient manufacturing processes that are

F. Nikbakhtnasrabadi, E. S. Hosseini, S. Dervin, D. Shakthivel, R. Dahiya
Bendable Electronics and Sensing Technologies (BEST) Group
University of Glasgow
Glasgow G12 8QQ, UK
E-mail: ravinder.dahiya@glasgow.ac.uk

 The ORCID identification number(s) for the author(s) of this article can be found under <https://doi.org/10.1002/aelm.202101348>.

© 2022 The Authors. Advanced Electronic Materials published by Wiley-VCH GmbH. This is an open access article under the terms of the Creative Commons Attribution License, which permits use, distribution and reproduction in any medium, provided the original work is properly cited.

DOI: 10.1002/aelm.202101348

Another challenge with wearable sensors-based approach is that an increasing number of devices (e.g., different types of sensors, data transmission devices etc.) are being explored to monitoring several health parameters, which raises integration related challenges, higher cost, and power requirements. Furthermore, user comfort could also be affected. In this regard, the multifunctional antennas (e.g., as sensor along with typical wireless communication function) offer an interesting solution.^[20–22] For example, an antenna has been used as wireless temperature sensor by replacing a section of track with the temperature sensitive material such as poly(3,4-ethylenedioxythiophene polystyrene sulfonate).^[16] Likewise, the geometry (e.g., serpentine structures) or physical features of substrates (e.g., stretchability) have been exploited to modulate the resonant frequency of the antenna and hence use them as strain or pressure sensors.^[22] This approach could be further advanced by using functional substrates and exploiting their inherent features. For example, piezoelectric materials as substrates could offer new capability to measure the dynamic pressure to monitor the biological signals.^[23,24] In relation with wearable systems, the piezoelectric polymers such as Polyvinylidene fluoride (PVDF) and Poly L-lactic acid (PLLA) are attractive due to their high chemical stability, flexibility, and biocompatibility. In fact, PLLA has an advantage for pressure sensing as unlike PVDF it does not exhibit pyroelectricity and hence there is no interference due to temperature. Further, the biodegradability of PLLA makes it attractive for both in vitro and in vivo implantable applications.^[25] Considering such attractive features, herein we have used PLLA nanofibers-based substrate for sensor development.

In this work, an interdigitated capacitive (IDC) sensor is developed on electrospun PLLA nanofibers-based substrate and connected in parallel with a planar inductor forming a LC circuit to realise wireless pressure sensor. The LC circuits is designed to resonate at about 13.56 MHz. The IDC configuration of the sensor offers long stability, high accuracy, and lower power consumption with respect to typical parallel plate capacitors (PPC).^[26,27] Further, it is easier to develop IDC with resource-efficient printing methods such as screen printing.

The PLLA nanofibers-based substrate used here, to realise the IDC capacitive sensors, offers better conformal contact with the skin and improves sensitivity under the pressure due to its piezoelectric property. It provides a direct interaction between the sensing elements and environment.^[28] Moreover, due to the unipolarization of PLLA nanofibers during electrospinning, change in the permittivity of the dielectric layer is expected in response to applied pressure, which allows linear responses of capacitive response over a wide range of 0–16 kPa. This pressure range is of the same order as one used in commercial bandages for compression therapy and therefore, we have integrated the presented LC tank-based sensor on a compression bandage to demonstrate its potential use in the online monitoring of sub-bandage pressure. The application of optimum pressure by the bandage, together with the electroceutical arrangement facilitated by the piezoelectric PLLA substrate, could accelerate the cell regeneration and hence wound healing. The wireless mechanism of presented sensor is based on inductive coupling in near field region. The application of external pressure leads to changes in the capacitance of IDC on PLLA substrates, and thus the resonant frequency of the LC circuit is altered as a function of applied pressure. The sensing data are encoded through backscattering power without using an IC to record and process data. The electrospinning and screen-printing, used here to develop entire sensor, offers a unique possibility for low-cost and mass production of devices with high reproducibility.

2. Experimental Section

2.1. Fabrication of PLLA Nanofibers

A 4 wt% PLLA solution was prepared by dissolving PLLA pellets (Corbion, The Netherlands) in a 1:4 ratio dimethylformamide and Dichloromethane (DCM) (Sigma-Aldrich, UK) mixed solvent for 10 h. The solution was stirred at room temperature by a magnetic stir bar at 300 rpm (Figure 1a). The multilayered membrane of the PLLA nanofibers mat, was fabricated by electrospinning of

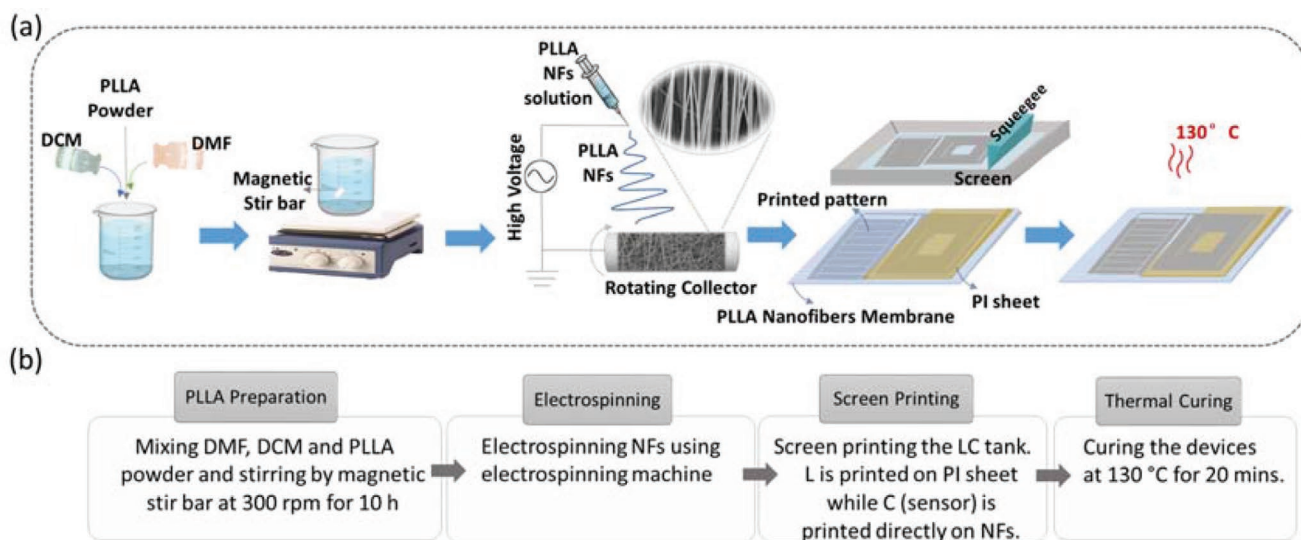


Figure 1. a) Schematic showing the fabrication of pressure sensor based on printed LC Tank on Electrospun PLLA Nanofibers. b) flowchart demonstrating fabrication procedure of the LC Tank.

Table 1. Physical dimensions of the IDC and planar inductor.

IDC		Inductor	
Parameter	Value [mm]	Parameter	Value [mm]
Length of fingers	20	Width of line	0.4
Width of fingers	0.5	Spacing	0.3
Number of fingers	40	Number of turns	15
Interspacing	0.4		

the PLLA polymer solution at 15 kV and a flow rate of 0.5 mL h⁻¹ with a drum speed of 3000 rpm (Figure 1b). The electrospun nanofibers were annealed in an oven at 100 °C for 4 h.

2.2. Sensor Design and Fabrication

Initially, the LC tank was simulated using the Advanced Design System (ADS) momentum simulator (Keysight Technologies, Santa Clara, CA). The LC tank consist of an interdigitated capacitor (IDC) connected in parallel with an inductor (L). These two elements are designed in a way that LC tank resonates at 13.56 MHz. **Table 1** summarized the physical dimensions of the LC tank. In simulation, dielectric constant of the PLLA substrate was considered as 3.5. Square-shape (1 cm) parallel plate printed capacitor that sandwiches a dielectric layer of the PLLA nanofibers with the thickness of 40 μm were fabricated to measure the dielectric constant of PLLA nanofibers. The approximate thickness of printed layers and surface roughness were considered in the simulation.

Figure 1 shows the fabrication steps for realising LC tanks using screen printing. Commercial stretchable silver paste (PE873, Dupont, UK.) with a sheet resistance of 110 mΩ sq⁻¹ was used to print the LC tank (Figure 1c). A bridge was also printed separately to make a connection between both ends of the inductor. The silver paste has good electrical conductivity in DC and high-frequency range and can be printed and cured over various polymeric substrates at low temperatures (i.e., 100–160 °C for 2–10 min) as mention in the datasheet.

The electrospinning method allows fabrication of a thin membrane of well-aligned PLLA nanofibers. The membrane is highly flexible and has a porous structure that can interact well with soft human tissue because of breathability, conformability, and nontoxic character. The silver paste used in this work, also has an appropriate viscosity to establish good adhesion with the nanofibers after thermal curing. The IDC, which is sensing element, was printed on the nanofibers, whereas the inductor was printed directly on a PI sheet. The sensing mechanism is based on the change in capacitance of the printed LC tank on PLLA nanofibers in response to applied pressure. Since the nanofibers have piezoelectric properties, only IDC is printed on PLLA nanofibers membrane to develop the pressure sensor. The inductor was printed on the PI sheet to isolate it from the electric charge generated by PLLA nanofibers. Thus, the effect of pressure on the performance of the coil antenna is negligible.

We also printed some inductors on PI sheet using inkjet method and noted that the quality factor of inkjet-printed inductor is much lower than the one realized using screen printing. In fact, the quality factor with 5 layers of inkjet printed inductor can be attained with just one layer of screen-printing structure. So, inkjet printing appears time consuming and costly compared to screen printing. Besides, the ink used for inkjet printing is less viscous compared to the paste used for screen printing. As a result, the inkjet printed structures may see the ink seeping through the PLLA nanofibers. In contrast, as the silver paste used for screen printing is high viscous such challenges were not experienced thus the current work was carried out by screen printing method. The screen printer employed is a semiautomatic screen-stencil printer (model C920, Aurel Automation, Italy) with a flat bed. The screen used to print the pattern is 400 mesh thread per centimeter (Figure 1c). The density of mesh is adequate to print a fine pattern with a resolution of about 100 μm. The bridge was also printed on the PI sheet to connect the inner end of the inductor to the capacitor using a conductive glue. After printing, the samples were cured in an oven for 20 min at 130 °C (Figure 1d). **Figure 2a** demonstrates the photograph of printed LC resonant

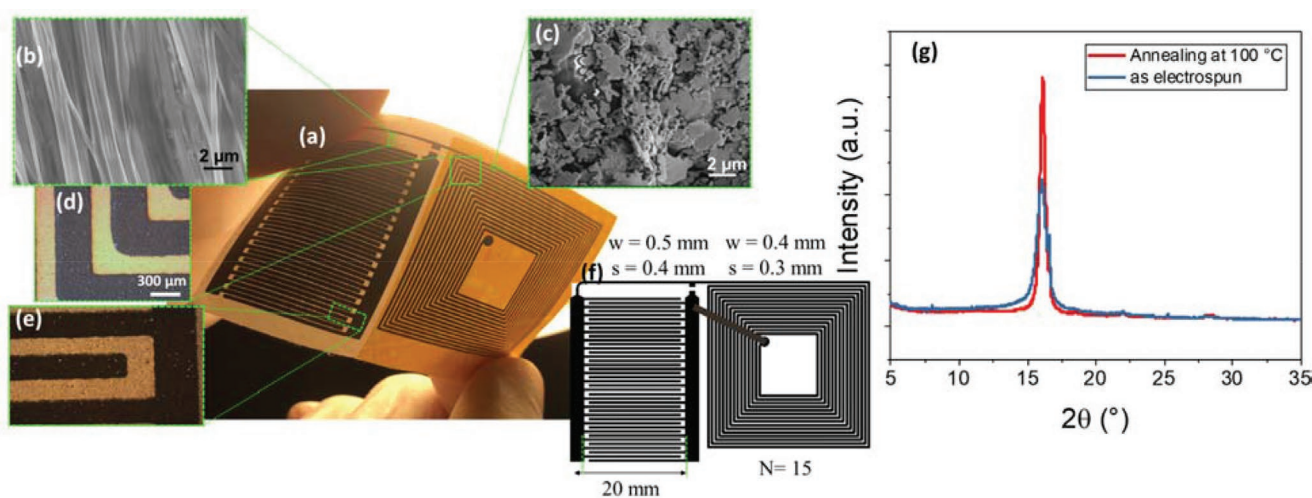


Figure 2. Screen-printed flexible LC tank: a) Photograph of the fabricated LC tank, b) SEM image of the PLLA nanofibers, c) SEM image of the stretchable silver paste consists of micrometer-scale silver flakes. d,e) Optical microscopy images of a finger of the IDC and the corner of inductor lines respectively. f) Schematic of the parallel LC tank. g) XRD pattern of electrospun and annealed PLLA nanofibers.

configuration consisting of the planar rectangle inductor connected in parallel to the IDC.

2.3. Materials and Sensor Characterization

The morphology of the piezoelectric PLLA nanofibers that are well aligned and densely packed (average diameter of 800 nm) is imaged using a high-resolution scanning electron microscope (SEM) (SU8240 Hitachi High-Tech) as shown in Figure 2b. The SEM image of the conductive composite paste (Figure 2c) shows the stretchable silver paste containing micrometer-sized silver flakes. The average thickness of the single-layer printed line on PI sheet was $10.83 \pm 0.65 \mu\text{m}$ with a conductivity of $1.1 \times 10^6 \text{ S m}^{-1}$. The optical microscopy images of a corner of inductor traces and the finger of IDC respectively in Figure 2d,e, show the resolution of screen-printed structures. Figure 2f shows the schematic of the parallel LC tank.

The crystallinity of the electrospun nanofibers was investigated using X-ray diffraction (XRD) (PANalytical X'Pert PRO MPD diffractometer). Figure 2g shows the XRD pattern graph of electrospun PLLA nanofibers before and after annealing. Only one sharp diffraction peak at 2 theta of about 16.5° was observed. This peak corresponds to the crystalline planes of (200) and (110) of PLLA and confirms the piezoelectric β -phase of PLLA nanofibers.^[29,30] The result confirms that the electrospinning process could control the crystalline structure of PLLA effectively by aligning molecular chains in the fibres. This is due to uniaxial stretching of polymer solution and the electric field applied during electrospinning process. The peak intensity and the crystallinity of nanofibers increased by annealing, as shown in Figure 2g.

Inductors and capacitors were characterized separately using an Agilent 4294A Precision Impedance Analyzer along with a 42941A impedance probe kit (Keysight Technologies, Santa Clara, CA). The capacitor was positioned and fixed to a 1004 miniature single point load cell. Pressures in wide range of 0–16 kPa were uniformly applied to the sensing capacitors using a load cell. A small rectangular glass slide as a moving plate has been used to apply the required pressure. This plate was controlled with a motorized stage with a resolution of $\approx 0.1 \text{ mm}$. The fixed and the moving plates were paralleled to guarantee a uniform contact pressure. Both plates were covered by a thin dielectric pad with relative permittivity close to 1 to prevent forming parallel plate capacitor between the moving plate and the sensing capacitor once they are in contact. The parameters of interest measured using an Agilent 4285A Precision LCR Meter were recorded using a custom-made LabVIEW program.

Tagformance Pro HF^[31] was used to characterise the LC tank by monitoring wirelessly the shift of resonance frequency and modified impedance of the reader antenna as a result of inductive coupling with the LC tank in response to applied pressure. Tagformance Pro is a measurement system for evaluating the performance of UHF RFID, HF RFID, and NFC transponders. The equipment works like a vector network analyser capable of measuring impedance and frequency responses when Passive Measurement is chosen in the measurement menu.

2.4. Cell Growth, Adhesion, and Proliferation on Electrospun PLLA Nanofibers

Human dermal fibroblast (adult) (HDFa) cells were used to assess the biocompatibility and suitability of the PLLA nanofibers as wound dressings. First, HDFa cells were cultured at 37°C in a 5% CO_2 incubator at log phase growth using Medium 106 (fibroblasts) complemented with a low serum growth supplement containing fetal bovine serum, basic fibroblast growth factor, heparin, hydrocortisone, and an epidermal growth factor. The cultured HDFa cells were then seeded on the electrospun PLLA nanofibers in 24 well plates at a cell density of 1×10^4 cells per sample. After a 1 h resting phase to allow cells to settle on the fibers, the desired volume of culture media was added to each well before incubating at 37°C in a 5% CO_2 incubator for 1, 3, and 5 days. The culture medium was replaced every 2 days.

Prior to incubation the electrospun PLLA nanofibers were cut into circular shapes that fit into the 24-well plates. The electrospun PLLA nanofibers were then immersed in 70% v/v ethanol for 12 h followed by washing with sterile phosphate buffer saline (PBS) (X3) and sterilized under UV light for 1 h on each side. Following sterilization, the electrospun PLLA nanofibers were hydrated by immersing the scaffolds in Medium 106 for 24 h at 37°C . After 1, 3, and 5 days of incubation, respectively, cell morphology attachment and growth were assessed using SEM microscopy (SU8240 Hitachi High-Tech). For this, HDFa cells grown on the electrospun PLLA nanofibers were rinsed with PBS (X3) and fixed using 2.0% glutaraldehyde in PBS at 5°C for 12 h. The fixed cell/nanofiber samples were then dehydrated by submerging each sample in a series of ethanol solutions (50%, 60%, 70%, 80%, 90%, and 100% ethanol, respectively) for 15 min and then air dried. Prior to SEM imaging the samples were Au coated.

3. Results and Discussion

3.1. Performance of Capacitive Sensor and Inductor

Three samples were fabricated following the procedure explained in the previous section. The IDCs were characterized using the Impedance Analyzer along with the impedance probe kit to cover frequency of interest (13.56 MHz) as well as self-resonant frequency. The self-resonant frequency was about 60 MHz which is much higher than the centre frequency. Figure 3a shows the $179 \pm 0.8 \text{ pF}$ capacitance of the IDC samples obtained at 13.56 MHz which is in good agreement with the simulated value (19 pF). It was observed that the capacitance was almost constant over 0 Hz–25 MHz frequency range. Since 13.56 MHz is far below the self-resonant frequency, and is within the region of flat response of the IDC can be used for application of pressure. The pressure sensing principle relies on the fact that the applied pulse pressure leads to the capacitance change. The change in capacitance will shift the resonance frequency of the parallel inductor, which can be monitored wirelessly through the inductive coupling with an external reader coil. Figure 3b shows the capacitor response when various pressure applied on the surface of the IDC using a load cell at a frequency of 1 Hz. The change in capacitance

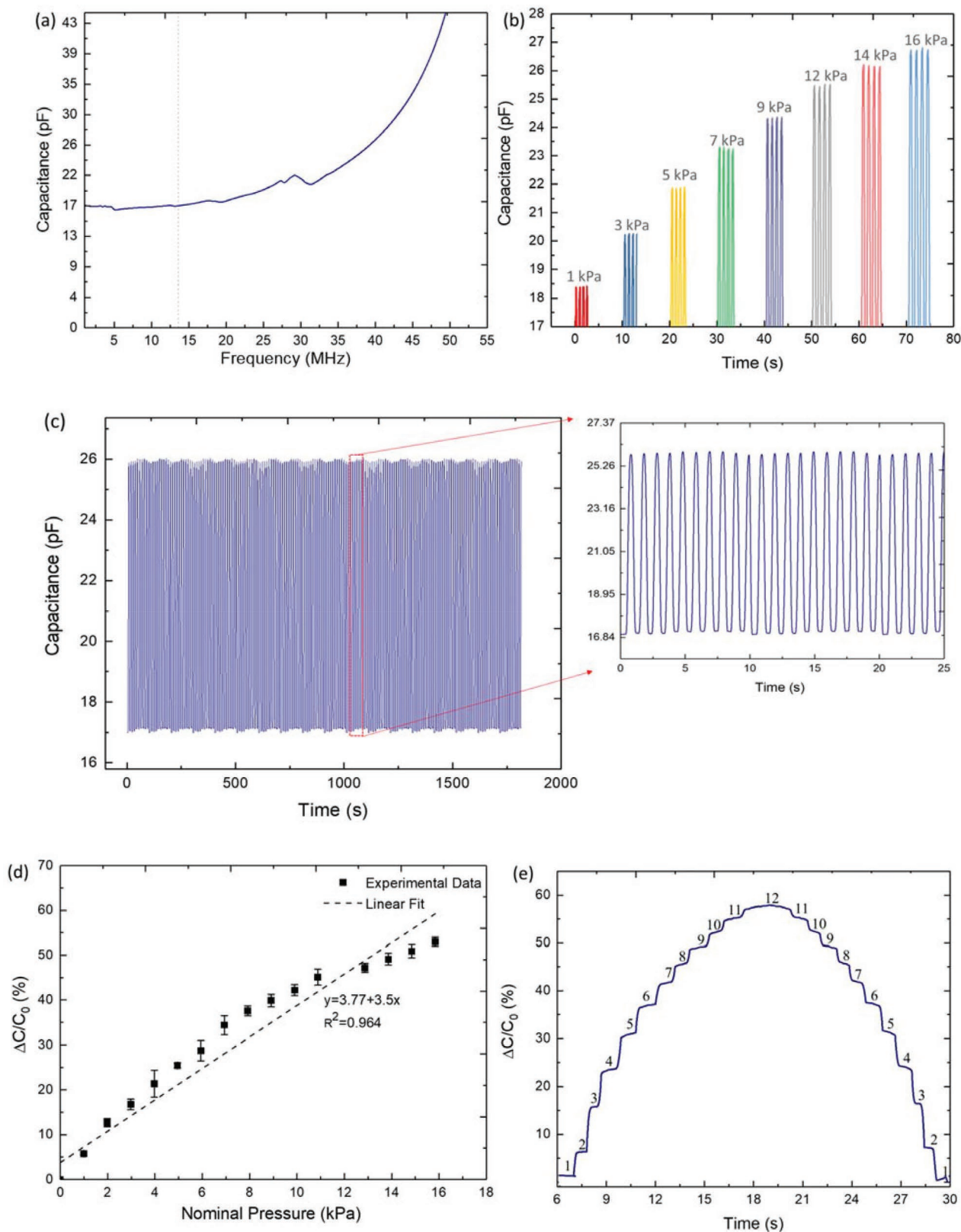


Figure 3. a) Frequency response of the interdigitated capacitor with sweep from 4 Hz to 55 MHz. b) Response of the IDC to various pressure values at 1 Hz. c) Cyclic response (over 1800 cycles) of the IDC to 14 kPa pressure, showing the durability and stability of the device (inset shows the 25 s of the capacitance response after 1000 cycles). d) The capacitance variation and sensitivity of the IDC to pressure variation. e) Capacitance response of the IDC to stepwise loading–unloading pressure from 0 to 12 kPa.

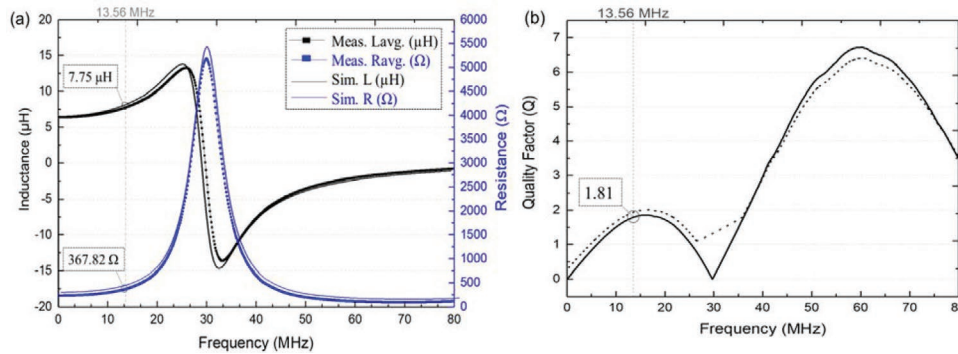


Figure 4. a) Measured and simulated frequency response of the screen-printed inductors in terms of average inductance and average resistance. b) Measured and simulated (dots) quality factor of printed inductor.

was constant and stable at each pressure values, which were repeated four times. To evaluate if the change in capacitance is due to the PLLA piezoelectric substrate, several capacitors were also printed on PI sheet and no notable capacitance change was observed in response to applied pressure. To demonstrate the durability and robustness of fabricated sensors, they were also subjected to loading–unloading cyclic pressure for up to 1800 cycles at 14 kPa. As shown in Figure 3c, the sensor exhibited a long fatigue life with stable variation under cyclic loading and releasing. Figure 3d shows the change of the capacitance of IDC as a function of applied pressure for three fabricated sensors. The low variation of the response among these sensors confirms the uniformity attained with the controlled fabrication process described above. The sensitivity of presented piezoelectric IDC was calculated with normalized change of capacitance divided by the nominal applied pressure $((\Delta C/C_0)/\Delta P)$. As shown in Figure 3d, the capacitance variation of the IDC increases linearly under the applied pressure with an average sensitivity of almost 3.5 Pa^{-1} . The capacitance response of the IDC to stepwise loading–unloading pressures (from 0 to 12 kPa) in Figure 3e shows the outstanding reliability with negligible hysteresis effect.

The inductors also were characterized using the Impedance Analyzer along with the impedance probe kit. The measured average value of the inductance ($7.75 \pm 0.14 \text{ } \mu\text{H}$) at resonance frequency (13.56 MHz) is close to the simulated value (7.8 μH). The average value of resistance at that frequency was $367.42 \pm 25 \text{ } \Omega$ (see Figure 4a). The slight deviation of resistance could be mainly due to the surface roughness of printed paste. The average quality factor achieved is 1.81, as shown in Figure 4b. The measured value is in good agreement with the simulation at 13.56 MHz. The quality factor of printed inductors is compared with conventional copper inductors with the same geometrical parameters and thickness of metal obtained through ADS simulation. This resulted in the quality factor of 65.72, which is far higher than the printed coil in the current work.

3.2. Response of LC tank

The resonant frequency of the RLC circuit is given by Equation (1)

$$f_{\text{res}} = \frac{1}{2\pi} \sqrt{\frac{1}{LC} - \left(\frac{R}{L}\right)^2} \quad (1)$$

Where R represents the resistance of the printed coil antenna, and L and C represent the inductance and capacitance of the planar antenna coil and the interdigitated capacitor, respectively. It is noted that the unlike conventional coils (made of copper) the resistance in present case is not negligible. The self-resonant frequency is much higher than the working frequency, so the parasitic capacitance of the coil antenna does not affect the resonant frequency of the LC tank.

A 50 Ω SMA (SubMiniature version A) connector was glued to the LC tanks. A robust connection was provided using silver epoxy adhesive (Mg Chemicals), which is curable at room temperature. Prior to measurement, calibration was performed using 50 Ω terminator and open load following the software instructions. The termination is included in the Tagformance Pro HF kit. Figure 5a shows the resistance and reactance of the parallel LC tank. The LC circuit impedance is given by Equation (2).

$$Z_{\text{LC}} = R_{\text{LC}} + j X_{\text{LC}} = R + j \left(\omega L - \frac{1}{\omega C} \right) \quad (2)$$

The LC tank resonates at around 13.61 MHz, which is close to the value obtained from the simulation (Figure 5a). In order to consider quality factor as sensing inductor, change in quality factor in response to applied pressure has been evaluated (Figure 5b). The quality factor is defined as f_{res}/BW , where the f_{res} is centre frequency and $BW = |f_2 - f_1|$ which for the proposed LC tank is 648 kHz. The quality factor fluctuates around the initial value; thus, it does not demonstrate a linear trend in response to applied pressure.

3.3. Inductive Telemetry System

The change in capacitance of the pressure sensor can be measured wirelessly using the modified reflected impedance of inductively coupled reader antenna (external coil). To this end, prior to measurement of S_{11} and modification of impedance of reader antenna inductively coupled with LC tank, a reference measurement was carried out to measure S_{11} of the reader

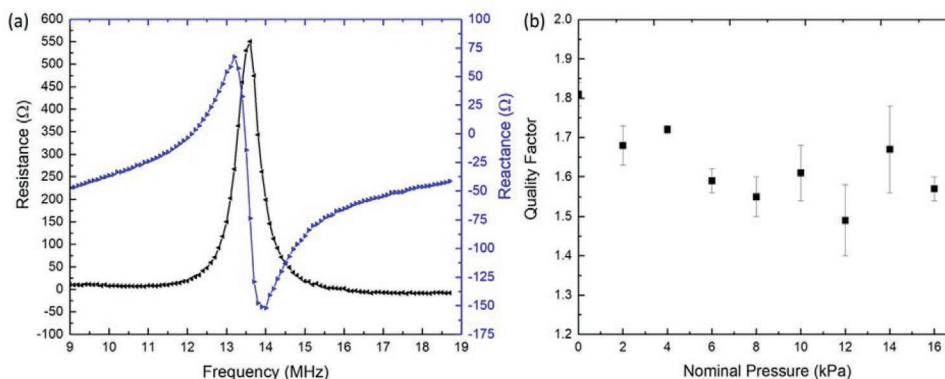


Figure 5. a) measured resistance and reactance of the LC tank. b) Quality factor of the LC tank in response to various applied pressure.

antenna itself to obtain its frequency response. This is used to calculate the normalized responses where the impedance of the reader itself is subtracted. The reader antenna is Voyantic C60 that is included in the Tagformance Pro HF kit. **Figure 6a** demonstrates the set-up comprising of the Tagformance Pro unit connected to the reader antenna and measurement software running on a computer. Voyantic C60 is a loop antenna (diameter 60 mm) consisting of four turns. These measurements were carried out when the distance between the LC tank and reader antenna was fixed as 16 mm. This gap is suggested by Voyantic as an optimal measurement distance to use the system. It is important to retain the distance since it has an impact on the coefficient of coupling between the two coils. The frequency range was set from 10 to 30 MHz with 10 kHz resolution bandwidth, which covers the resonant frequency of the LC tank as well as sufficient margin as the resonant frequency shifts due to applied pressure. The transmit power was set to 0 dBm.

The wireless response of the LC tanks was evaluated in response to applied pressure on IDC capacitor using the load cell. The C60 antenna was used to wirelessly measure change in reflected impedance of reader coil and resonant frequency. The impedance measured at the reader coil is equivalent to resistance (R_r), inductance (L_r), and tuning capacitance (C_{tune}) of the reader antenna and the reflected impedance of the sensing LC tank as described in Equation (3). M is the mutual inductance between two coupled coils.

$$Z(\omega) = R + jX = R_r + j\omega L_r + \frac{1}{j\omega C_{\text{tune}}} + \frac{(\omega M)^2}{Z_{\text{LC}}(\omega)} \quad (3)$$

As reference measurement was done prior to this measurement, the impedance of the C60 antenna is subtracted in the response. So, the last term (i.e., $\frac{(\omega M)^2}{Z_{\text{LC}}(\omega, P)}$) of Equation (3) represents the normalized impedance change corresponding to the applied pressure.

Various pressure (0–16 kPa) were applied on the capacitor at a frequency of 1 Hz. Once the magnetic field from the reader antenna is received by the LC tank, the shift of resonant frequency is considered as an indicator of applied pressure. The normalised resistance and reactance of the printed tank for

various pressure is shown in Figure 6a,b, respectively. The relation between change of impedance and resonant frequency shift is shown in Figure 6d,e as a function of applied pressure. The effect of applied pressure can be seen in both magnitude (Figure 6d) and phase (Figure 6e) of frequency response. Figure 6f shows the linear curve fitting can represent the shift of resonance frequency, while the pressure is increasing. Both magnitude and phase follow almost similar trend. However, the phase parameter expresses more reliable result as the standard deviation of various samples is negligible. The magnitude and phase of the resonance frequency decreases linearly by $0.1 \pm 0.08 \text{ kHz Pa}^{-1}$ and $0.11 \pm 0.02 \text{ kHz Pa}^{-1}$, respectively in the range from 0 to 16 kPa. **Table 2** compares the response of our sensor with some relevant capacitive sensors reported for pressure monitoring (wired and wireless techniques). Among capacitive sensors reported for in kPa range operation, our sensor demonstrates highest sensitivity ($(\Delta C/C_0)/\Delta P$). Wireless performance also is good, considering that the frequency shift at reader depends on the mutual inductance and quality factor of the two coils. Since our coil is printed the quality factor is lower than the coils fabricated by metal traces. Thus, our sensor also demonstrates a good sensitivity to the pressure, in comparison with other nonprinted and nonflexible wireless sensors.

3.4. Biocompatibility: Cell Growth, Adhesion, and Proliferation on Electrospun PLLA Nanofibers

SEM imaging was used to examine the cell growth, adhesion, and proliferation of HDFa cells grown on the electrospun PLLA nanofibers. As can be observed from **Figure 7**, the attachment of HDFa cells to the PLLA substrates is prominent after 24 h. The attached cells then started to noticeably spread across the scaffolds provided by the electrospun PLLA nanofibers, forming a monolayer like structure intercellular connections, and thus indicative of the strong cytoskeleton stretching. The observed cell behaviors on the electrospun PLLA nanofibers therefore confirm that the nanofibrous scaffolds facilitate cell adhesion/attachment and proliferation due to their porosity and high surface area and hence are suitable to accelerate the wound healing.

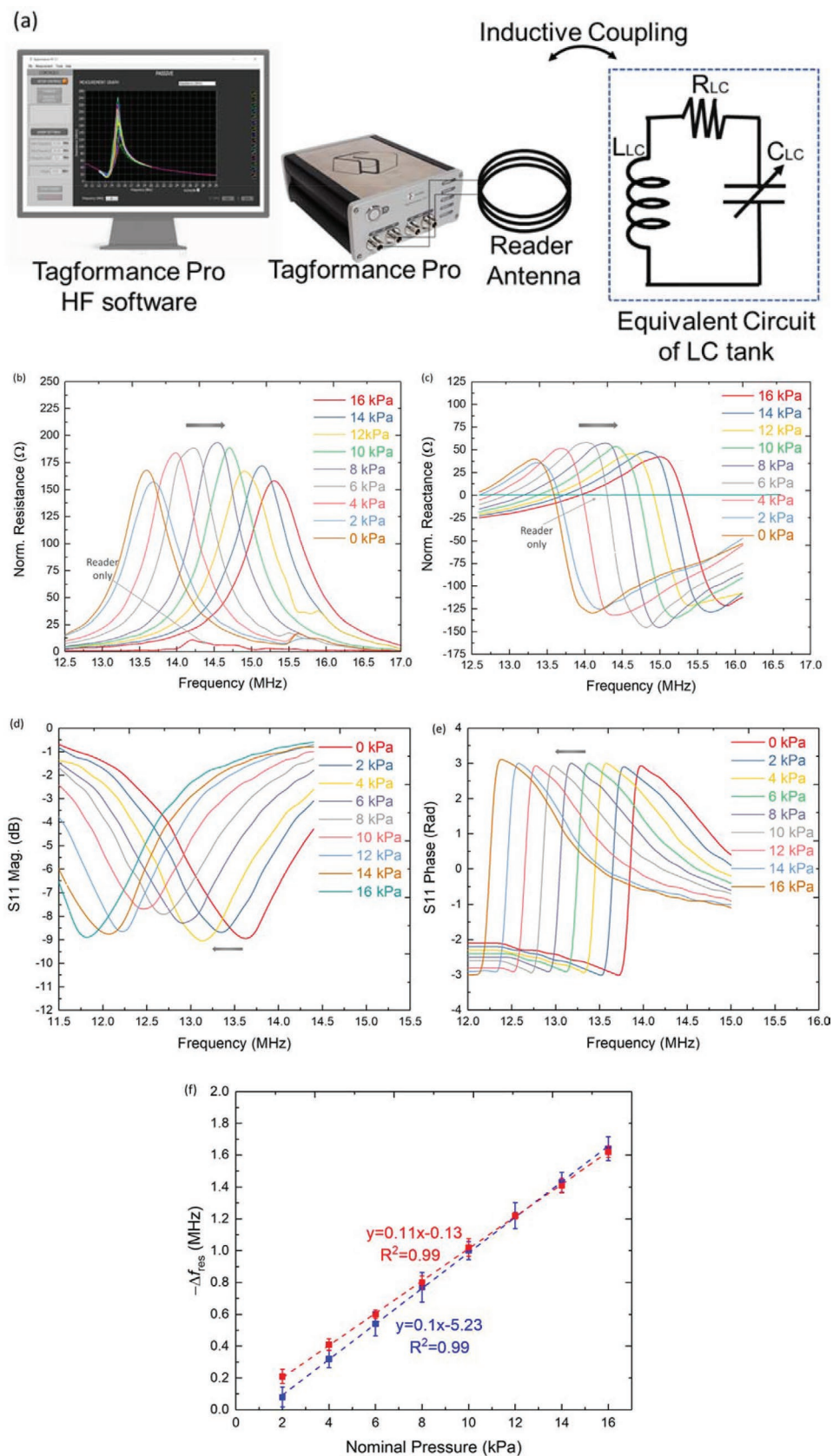


Figure 6. a) Schematic of the setup for near-field communication and power transfer for HF RFID tags using Tagformance. Change in reader coil response associated with applied pressure: b) normalized impedance and c) normalized reactance. d) frequency response of the reader coil, e) reflection coefficient phase shift, f) comparison of frequency change considering magnitude and phase of the reader antenna.

Table 2. Comparison between some capacitive pressure sensors.

Sensing material	Type of capacitor	Pressure range	Sensitivity		Frequency range	Wireless	Reference
			$(\Delta f_{res})/\Delta P$	$(\Delta C/C_0)/\Delta P$			
Pyramid Microstructure PDMS	PPC	0–26 kPa	–2030 Hz/kPa	–	≈725–800 MHz	Yes	[32]
Boron-doped silicon diaphragm	PPC	0–6.6 kPa	900 Hz/kPa	–	95–103 MHz	Yes	[33]
Single layer graphene	Coplanar IDC	0.11–80 kPa	–	0.01 kPa ^{–1}	N/A	No	[27]
sandpaper-molded carbon nanotube/ PDMS composite	PPC	<5 Pa	–	9.5 kPa ^{–1}	N/A	No	[34]
PVA-PDMS	PPC	50 kPa	–	4 MPa ^{–1} at 0.1 kPa	N/A	No	[35]
Pure PVDF nanofibers	PPC	1–6 kPa	–	0.02 kPa ^{–1}	N/A	No	[36]
PLLA electrospun nanofibers	IDC	0–16 kPa	1200 Hz/kPa	0.035 kPa ^{–1}	≈11–14 MHz (HF band)	Yes	This work

4. Application in Wearable Healthcare Systems

The proposed LC tank sensor has potential application in accelerated wound healing and compression therapy. Compression therapy is an action of applying controlled pressure to the affected limb. Compression bandages are designed to boost blood flow and hence accelerate the wound healing. It also can be used to maintain constant pressure. There are several methods to apply negative pressure over the tissue^[37]; however, it is crucial to monitor the extent of the applied pressure in a noninvasive method to improve the effectiveness of therapy. Swelling and bruising are very common side effects in pressure therapy techniques for which there is no accurate control over the applied pressure and can increase the risk of further harm. Thus, wireless pressure sensor worn under the compression bandage or integrated on the bandage to monitor regularly the pressure applied on the wound could be an interesting noninvasive solution for the patients with chronic wounds. As shown above the fabricated sensor showed linear sensitivity and repeatability in the pressure range of 0–16 kPa (0–120 mmHg) which covers the pressure range reported for compression therapy.^[38] Further, the performance of the developed wireless sensor was evaluated by placing it under a commercial compression bandage worn by an healthy adult volunteer around the elbow of healthy women wearing the sensor under a commercial compression bandage (#1523, Molnlycke) (see **Figure 8b,c**; and Videos S1 and S2, Supporting Information). Four layers of the bandage were worn in a carefully controlled manner. **Figure 8a** shows the capacitance change and resonant frequency (wireless) upon tightening the compression bandage. The modified Laplace equation is used to calculate a gradual increase in pressure on the sensor over the clinically applicable range of pressures.^[39,40] According to the Laplace law, the applied pressures

by a bandage are a direct function of the number of layers and the tension of the bandage fabric itself, but reverse function to the width of the bandage circumference of the limb.^[39] These results show the possibility of predicting the pressure from the shift of frequency of reader antenna, provided the elasticity of the bandage and size of the limb are known. The reader coil in presented test can be substituted by a customized reader with a narrow bandwidth which can discriminate the different pressure ranges.

Since compression bandages are in close contact to human body the change in temperature of the body may affect the performance of the capacitive sensor. In this regard, the capacitance of the sensor was monitored with temperature increasing gradually from 25 to 40 °C. For this purpose, the sample was mounted on the PE120 stage (Linkam, UK) and the capacitance was recorded using a LCR meter controlled by a LABVIEW program. The temperature was increasing by 1 °C each time. Only 2% change in capacitance was observed during this experiment. However, once the temperature was stabilized it reached to the original value. So, the performance of the capacitive sensor is very stable even in the case of any change in the human body temperature.

For some applications (e.g., wound healing), the proposed sensor can be in direct contact with an open wound thus the substrate should be biocompatible. To ensure the biocompatibility of the PLLA nanofibers and evaluate their suitability as wound dressings the morphology, attachment, and growth of HDFa cells was examined after 1, 3, and 5 days of culture using scanning electron microscopy. SEM analysis revealed the attachment, growth, and migration of the HDFa cells along the well-aligned axes of the PLLA nanofibers with no sign of cytotoxic effect. Since PLLA nanofibers are biocompatible, the LC tank can be worn on the skin without the risk of skin agitation.

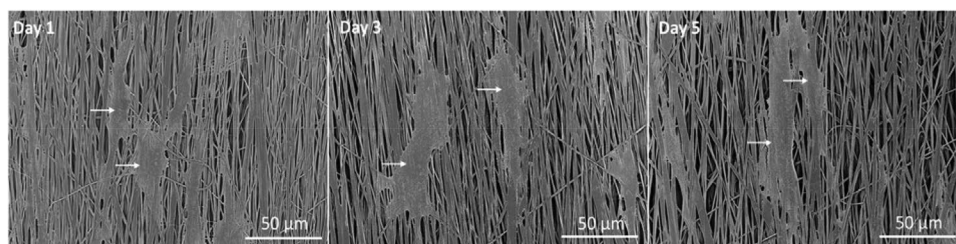


Figure 7. SEM images of HDFa cells cultured on well-aligned PLLA nanofibers after 1, 3, and 5 days.

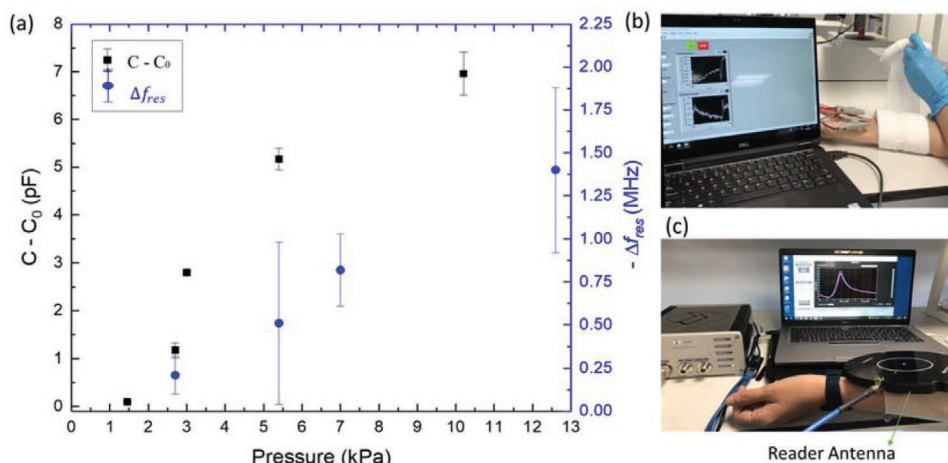


Figure 8. Potential application for the proposed LC tank to monitor pressure of compression bandage. a) change of capacitance and frequency as a function of applied pressure. b) Setup to test the LC tank under compression bandage (with wire). The result was obtained using LCR meter controlled by a LABVIEW program. c) Wireless setup to test the LC tank set under a compression bandage.

Furthermore, some research suggests that the PLLA can promote wound healing by preventing bacterial infections^[41] due to its piezoelectric nature.

5. Conclusions

In summary, we have developed a screen-printed flexible LC tank device to wirelessly detect the pressure and have showed its suitability for biomedical application. The presented sensor is developed using low-cost and scalable fabrication methods, such as electrospinning and screen-printing. The tank consists of a planar inductor connected in parallel to an interdigital capacitor designed to resonate at 13.56 MHz. The sensing principle is based on the change in the capacitance of IDC under pressure which leads to a variation in resonant frequency. The shift of frequency of the parallel LC tank as a measure for applied dynamic pressure is detected wirelessly using the inductive coupling with a second external inductor. The realised capacitive sensor exhibit high sensitivity 0.035 kPa^{-1} and 1200 Hz kPa^{-1} in wireless characterisation, along with excellent durability over 1800 cycles. The fabricated sensor demonstrated good repeatability and linear sensitivity in the pressure range (0–16 kPa) appropriate for wearable healthcare applications, such as monitoring the sub-bandage pressure. The application of optimum pressure by the bandage, together with the electrochemical arrangement facilitated by the piezoelectric PLLA substrate, could accelerate the cell regeneration and hence wound healing. An in-depth analysis of the influence of piezoelectric properties of PLLA on the wound healing through electrical stimulation will be explored further as a future work.

Supporting Information

Supporting Information is available from the Wiley Online Library or from the author.

Acknowledgements

This work was supported in part by Engineering and Physical Sciences Research Council through Engineering Fellowship for Growth (EP/R029644/1) and North West Centre for Advanced Manufacturing project funded by the European Union's INTERREG programme (H2020-Intereg-IVA5055), managed by the Special EU Programmes Body. The views and opinions in this document do not necessarily reflect those of the European Commission or the SEUPB.

Conflict of Interest

The authors declare no conflict of interest.

Data Availability Statement

The data that support the findings of this study are available from the corresponding author upon reasonable request.

Keywords

chipless LC tank, electrospinning, piezoelectric nanofibers, PLLA, wearable pressure sensor

Received: December 11, 2021

Revised: January 19, 2022

Published online: February 19, 2022

- [1] R. Dahiya, N. Yogeswaran, F. Liu, L. Manjakkal, E. Burdet, V. Hayward, H. Jörntell, *Proc. IEEE* **2019**, *107*, 2016.
- [2] J. R. Windmiller, J. Wang, *Electroanalysis* **2013**, *25*, 29.
- [3] W. Gao, S. Emaminejad, H. Y. Y. Nyein, S. Challa, K. Chen, A. Peck, H. M. Fahad, H. Ota, H. Shiraki, D. Kiriya, *Nature* **2016**, *529*, 509.
- [4] M. Zhu, Y. Wang, M. Lou, J. Yu, Z. Li, B. Ding, *Nano Energy* **2021**, *81*, 105669.
- [5] M. Zhu, M. Lou, J. Yu, Z. Li, B. Ding, *Nano Energy* **2020**, *78*, 105208.

- [6] P. Escobedo, M. Bhattacharjee, F. Nikbakhtnasrabadi, R. Dahiya, *IEEE Internet Things J.* **2021**, *8*, 5093.
- [7] W. Dang, L. Manjakkal, W. T. Navaraj, L. Lorenzelli, V. Vinciguerra, R. Dahiya, *Biosens. Bioelectron.* **2018**, *107*, 192.
- [8] Y. Wang, M. Zhu, X. Wei, J. Yu, Z. Li, B. Ding, *Chem. Eng. J.* **2021**, *425*, 130599.
- [9] P. Descent, R. Izquierdo, C. Fayomi, in *2018 Proc. IEEE Int. Symp. Circuits Syst.*, Florence, May **2018**.
- [10] M. Kaisti, T. Panula, J. Leppänen, R. Punkkinen, M. J. Tadi, T. Vasankari, S. Jaakkola, T. Kiviniemi, J. Airaksinen, P. Kostiaainen, *NPJ Digit. Med.* **2019**, *2*, 39.
- [11] N. Yogeswaran, E. S. Hosseini, R. Dahiya, *ACS Appl. Mater. Interfaces* **2020**, *12*, 54035.
- [12] M. Bariya, H. Y. Y. Nyein, A. Javey, *Nat. Electron.* **2018**, *1*, 160.
- [13] T. R. Ray, J. Choi, A. J. Bandodkar, S. Krishnan, P. Gutruf, L. Tian, R. Ghaffari, J. A. Rogers, *Chem. Rev.* **2019**, *119*, 5461.
- [14] Z. Yan, L. Wang, Y. Xia, R. Qiu, W. Liu, M. Wu, Y. Zhu, S. Zhu, C. Jia, M. Zhu, *Adv. Funct. Mater.* **2021**, *31*, 2100709.
- [15] M. C. Caccami, G. Marrocco, *IEEE Trans. Antennas Propag.* **2018**, *66*, 2779.
- [16] M. Bhattacharjee, F. Nikbakhtnasrabadi, R. Dahiya, *IEEE Internet Things J.* **2021**, *8*, 5101.
- [17] H. El Matbouly, S. Tedjini, K. Zannas, Y. Duroc, *IEEE J. Radio Freq. Identif.* **2019**, *3*, 83.
- [18] A. Palmroth, T. Salpavaara, P. Vuoristo, S. Karjalainen, T. Kääriäinen, S. Miettinen, J. Massera, J. Lekkala, M. Kellomäki, *ACS Appl. Mater. Interfaces* **2020**, *12*, 31148.
- [19] J. Koo, M. R. MacEwan, S.-K. Kang, S. M. Won, M. Stephen, P. Gamble, Z. Xie, Y. Yan, Y.-Y. Chen, J. Shin, *Nat. Med.* **2018**, *24*, 1830.
- [20] C. Occhiuzzi, S. Caizzone, G. Marrocco, *IEEE Trans. Antennas Propag.* **2013**, *55*, 14.
- [21] S. Manzari, C. Occhiuzzi, S. Nawale, A. Catini, C. Di Natale, G. Marrocco, *IEEE Sens. J.* **2012**, *12*, 2851.
- [22] F. Nikbakhtnasrabadi, H. El Matbouly, M. Ntagios, R. Dahiya, *ACS Appl. Electron. Mater.* **2021**, *3*, 2233.
- [23] S. O'Callaghan, P. Galvin, C. O'Mahony, Z. Moore, R. Derwin, *J. Wound Care* **2020**, *29*, 394.
- [24] E. S. Hosseini, S. Dervin, P. Ganguly, R. Dahiya, *ACS Appl. Bio Mater.* **2021**, *4*, 163.
- [25] S.-D. Yoon, Y.-S. Kwon, K.-S. Lee, *Int. Neurorol. J.* **2017**, *21*, 48.
- [26] A. Sutono, D. Heo, Y.-J. E. Chen, J. Laskar, *IEEE Trans. Microw. Theory Tech.* **2001**, *49*, 1715.
- [27] C. G. Núñez, W. T. Navaraj, E. O. Polat, R. Dahiya, *Adv. Funct. Mater.* **2017**, *27*, 1606287.
- [28] F. Molina-Lopez, T. Kinkeldei, D. Briand, G. Tröster, N. F. De Rooij, *J. Appl. Phys.* **2013**, *114*, 174907.
- [29] N. T. Cuong, S. Barrau, M. Dufay, N. Tabary, A. Da Costa, A. Ferri, R. Lazzaroni, J.-M. Raquez, P. Leclère, *Appl. Sci.* **2020**, *10*, 652.
- [30] E. J. Curry, K. Ke, M. T. Chorsi, K. S. Wrobel, A. N. Miller, A. Patel, I. Kim, J. Feng, L. Yue, Q. Wu, *Proc. Natl. Acad. Sci. USA* **2018**, *11*, 5909.
- [31] Tagformance Pro manual, <https://voyantic.com/products/tagformance-pro>, (accessed: September 2021).
- [32] W.-J. Deng, L.-F. Wang, L. Dong, Q.-A. Huang, *IEEE Sens. J.* **2018**, *18*, 4886.
- [33] O. Akar, T. Akin, K. Najafi, *Sens. Actuators, A* **2001**, *95*, 29.
- [34] S. G. Yoon, B. J. Park, S. T. Chang, *ACS Appl. Mater. Interfaces* **2017**, *9*, 36206.
- [35] R. Mikkonen, A. Koivikko, T. Vuorinen, V. Sariola, M. Mäntysalo, *IEEE Sens. J.* **2021**, *21*, 26286.
- [36] X. Yang, Y. Wang, X. Qing, *Sens. Actuators, A* **2019**, *299*, 111579.
- [37] C. Huang, T. Leavitt, L. R. Bayer, D. P. Orgill, *Curr. Probl. Surg.* **2014**, *51*, 301.
- [38] J. Hafner, W. Lüthi, H. Hänssle, G. Kammerlander, G. Burg, *Dermatol. Surg.* **2000**, *26*, 481.
- [39] S. Thomas, *J. Wound Care* **2014**, *23*, 234.
- [40] Compression Measurement System, <https://www.vipmedikal.com.tr/wp-content/uploads/2016/02/PicoPress.pdf> (accessed: September, 2021).
- [41] H. Miyazaki, M. Kinoshita, A. Saito, T. Fujie, K. Kabata, E. Hara, S. Ono, S. Takeoka, D. Saitoh, *Wound Repair Regen.* **2012**, *20*, 573.